SIMULATION OF FLOW WITHIN THE DIFFERENT CAVITIES USING SST K-Ω TURBULENCE MODEL

Nehir Tokgoz[1] , Rahim Hassanzadeh[2*], Besir Sahin[3],

[1]Department of Energy Systems Engineering, Osmaniye Korkut Ata University, Osmaniye,Turkey
[2]Department of Mechanical Engineering, Urmia University of Technology, Urmia, Iran
[3]Faculty of Engineering and Architecture, Mechanical Engineering Department, Cukurova University, Adana, Turkey
r.hassanzadeh@uut.ac.ir, nehirtokgoz@osmaniye.edu.tr, bsahin@cu.edu.tr

ABSTRACT: This work is a three-dimensional investigation about the flow structure within three different cavities such as rectangular, triangular and semi-circular shapes using computational fluid dynamics. The present study is performed based on the Reynolds numbers of 1,000. The aspect ratio of all under consideration cavities is L/D=2. In order to simulate and study the flow characteristics, SST K-ω model is combined with Navier-Stokes equations and applied on the non-uniform multi-block grid systems based on the finite volume technique. For enhanced visualization, different time-averaged and instantaneous flow patterns are presented. Within the cavities three different vortex mechanisms including of primary, developing and corner vortices are observed. Examination of instantaneous flow data revealed that the rate of unsteadiness within the rectangular cavity is higher than two other cavities. Finally, it is stated that at Re=1,000, flow is two-dimensional with respect to stream-wise and normal directions.

Keywords: Cavity, Computational Fluid Dynamics (CFD), Finite volume method, SST K-ω, Vortex flow

*Corresponding author. Tel: +98-4433980251, E-mail: r.hassanzadeh@uut.ac.ir

1. INTRODUCTION

The flow over cavities is of great interests due to very different applications in the science and engineering such as solar collectors, turbine blades, flow inside ribbed tubes and channels, flow over aircraft hulls, weapon bays and many other applications. In the past decade, several numerical and experimental investigations were performed on the heat and fluid flow within the cavities. In general, flow over and within the cavities may be divided into three different main groups including of lid-driven cavities (Zhang et al. [1], Povitsky [2], Oueslati et al. [3], Guermond et al. [4]), thermally-driven cavities (Vasseur [5]), and shear-driven cavities. However, some of the articles may be a combination of two or three mentioned groups (Stefanovic and Stefan, [6]). With respect to the subject of this study, we present a history of previous works associated to shear-driven cavities. Various experimental and numerical researches were performed about the shear driven cavities. For example, Zdanski et al. [7] have numerically presented a physical analysis on the flow over cavities with large aspect ratio. They applied standard k-ε turbulence model at different Reynolds number corresponding to laminar and turbulent values. They have demonstrated that the vorticity shed at the upstream corner and stagnation region formed at the downstream vertical face has a major influence on vortices positioned inside the cavity. Saqr et al. [8] have computed the shear driven vortex flow in a cylindrical cavity using a modified k-ε turbulence model. They have compared their results with other measurements predicting the shear-driven vortex flow inside the cavity, successfully. Flow and heat transfer over rectangular shallow cavities at different aspect

ratios have performed by Mesalhy et al. [9] using standard k-ε turbulence model. It has been demonstrated that based on the value of the cavity aspect ratio, the type of cavity flow changes from open cavity flow to close cavity flow. They also found that the critical aspect ratio at which this change occured was seven, approximately. On the other hand, an experimental measurement of flow past cavities of different shapes has conducted by Ozalp et al. [10]. In their research, three different cavity shapes including of rectangular, triangular, and semi-circular cavities were under consideration at three Reynolds numbers of 1230, 1460 and 1700. Their results have revealed that in addition to cavity shapes, changing of Reynolds number has some degree of influence on the structure of flow and turbulence quantities. They also have stated that maximum Reynolds stress and turbulence intensity values were observed in the lid section of the cavity at the centerline position and rectangular and triangular cavities cause much greater turbulence compared to the semi-circular cavity shape.

Most of investigations in open literature associated to square and/or rectangular cavities while there are many various applications in which the non-rectangular cavities such as triangular and semi-circular are used. This study is focused on the flow structure within the three different cavities such as rectangular, triangular, and semi-circular shapes using shear stress transport (SST) k-ω turbulence model. It is assumed that the length of cavities is infinite with respect to the spanwise direction. In the past decade, different numerical methods were used for simulation and solution of flow within the cavities (Ho and Lin [11], Wei et al. [12], Gupta and Kalita [13], Peng and Davidson [14], Zdanski et al. [7], Diang et al. [15]). For this reason, the validity of this turbulence model during the present case study is under consideration.

2. FLOW DOMAIN AND BOUNDARY CONDITIONS

In the present three-dimensional study, three different cavity shapes such as rectangular, triangular, and semi-circular cavities are under the consideration. The aspect ratios (ratio of the cavity length, L, to the cavity depth, D,) are identical and equal to 2.0. Figure 1 shows the details of the flow domain dimensions and the applied grid systems. For simulation of flow structure a computational domain with dimensions in the range of $0 \leq x/L \leq 10$ in the stream-wise direction, $-1 \leq y/L \leq 1$ in the normal direction and $-0.5 \leq z/L \leq 2$ in the span-wise direction were used. The value of the Reynolds number with respect to the cavity depth and free-stream velocity is 1,000 corresponding to inlet velocity of 0.02 m/s. In order to compute the flow data, the multi-block grid system was constructed on the flow domain. For performing this construction, firstly the flow domain was divided into different blocks. After that, different grid sizes were applied on the blocks in which the finer grids are associated to the regions inside the cavities and coarse grids are associated far from the cavities (free-stream flow). The total number of control volumes is indicated in table 1.

Table 1: Details of total grids used in the present study

	Number of control volumes	Minimum grid size*
Rectangular cavity	695,700	0.006D
Triangular cavity	654,450	0.006D
Semi-circular cavity	1,096,788	0.006D

* D is the cavity depth

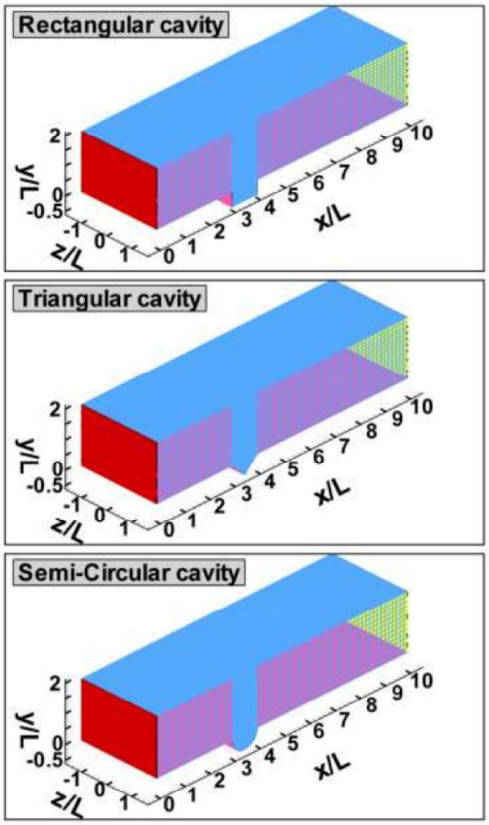


Figure 40. Details of Flow Domain And Applied Multi-Grids Topology

3. GOVERNING EQUATIONS AND NUMERICAL METHOD

3.1. Conservation of mass and momentum

The governing equations for incompressible and Newtonian fluid used in this study are summarized as following:

Conservation of mass:

$$\frac{\partial u_i}{\partial x_i} = 0 \tag{1}$$

Conservation of momentum:

$$\frac{\partial u_i}{\partial t} + \frac{\partial}{\partial x_j}\left(u_i u_j\right) = -\frac{1}{\rho}\frac{\partial p}{\partial x_i} + \nu \frac{\partial u_i}{\partial x_j \partial x_j} \tag{2}$$

where x_i=(x, y, z), u_i=(u, v, w), p and t are the coordinate space, velocity, pressure and time, respectively.

3.2. The shear stress transport (SST) k-ω turbulence model; an overview

The CFD model used in the present work is the Reynolds-averaged Navier-Stokes equations (RANS) model according to shear stress transport (SST) k-ω turbulence closure model developed by Menter [16]. The SST k-ω model is similar to the standard k-ω model, but includes three refinements. These refinements are; i-) This model incorporates a damped cross-diffusion derivative term in the ω equation, ii-) The definition of the turbulent viscosity is modified to account the transport of the turbulent shear stress and iii-) The model constants are different. There is no need for a special treatment for the viscosity affected wall region because of the low-Reynolds correction in the k-ω and k-ω SST models. The transport equations for k and ω may be written as (Dewan [17]):

$$\frac{\partial k}{\partial t}+\bar{u}_j\frac{\partial k}{\partial x_j}=\frac{\partial}{\partial x_j}\left[\left(\nu+\sigma_k\nu_t\right)\frac{\partial k}{\partial x_j}\right]+P_k-\beta^*k\omega \tag{3}$$

$$\frac{\partial \omega}{\partial t}+\bar{u}_j\frac{\partial \omega}{\partial x_j}=\frac{\gamma P_k}{\rho\nu_t}-\beta\omega^2+\frac{\partial}{\partial x_j}\left[\left(\nu+\sigma_{\omega 2}\nu_t\right)\frac{\partial \omega}{\partial x_j}\right]+2\left(1-F_1\right)\sigma_{\omega 2}\frac{1}{\omega}\frac{\partial k}{\partial x_j}\frac{\partial \omega}{\partial x_j} \tag{4}$$

The eddy viscosity is written as (Dewan [17]):

$$\nu_t=\frac{a_1 k}{\max\left(a_1\omega, SF_2\right)} \tag{5}$$

The auxiliary relations and the model constant can be written as (Dewan [17]):

$$F_1=\tanh\left(\left\{\min\left[\max\left(\frac{\sqrt{k}}{\beta^*\omega y},\frac{500\nu}{y^2\omega}\right),\frac{4\sigma_{\omega 2}k}{CD_{k\omega}y^2}\right]\right\}^4\right) \tag{6}$$

$$F_2=\tanh\left(\max\left(\frac{2\sqrt{k}}{\beta^*\omega y},\frac{500\nu}{y^2\omega}\right)^2\right) \tag{7}$$

$$P_k=\min\left(\tau_{ij}\frac{\partial \bar{u}_i}{\partial x_j},10\beta^*k\omega\right) \tag{8}$$

$$CD_{k\omega}=\max\left(2\rho\sigma_{\omega 2}\frac{1}{\omega}\frac{\partial k}{\partial x_i}\frac{\partial \omega}{\partial x_i},10^{-20}\right) \tag{9}$$

The constants for example Φ are blended using the relation (Dewan [17]):

$$\phi=\phi_1F_1+\phi_2\left(1-F_1\right) \tag{10}$$

$$\gamma_1=\frac{\beta_1}{\beta^*}-\frac{\sigma_{\omega 1}k^2}{\sqrt{\beta^*}},\qquad \gamma_1=\frac{\beta_2}{\beta^*}-\frac{\sigma_{\omega 2}k^2}{\sqrt{\beta^*}}$$

$$\beta_1=3/40,\qquad \beta_2=0.0828,\qquad \beta^*=9/100,\qquad \sigma_{k1}=0.85,\qquad \sigma_{k2}=1 \tag{11}$$

$$a_1=0.31,\qquad \sigma_{\omega 1}=0.5,\qquad \sigma_{\omega 2}=0.856$$

3.3. Solution procedure

A three-dimensional finite volume code was applied to discrete the 3D flow domain through a second order scheme. In order to discrete the convective terms, QUICK scheme was applied. Moreover, the SIMPLE algorithm was used to achieve the mass conservation between the pressure and velocity terms in the discretized momentum equation. On the other hand, for discretization of time a second order implicit method was employed. For inlet section and lower wall Dirichlet boundary conditions were applied while for outlet section as well as upper and side walls the Neumann boundary conditions were employed. Applications of symmetric conditions on the side walls indicate the infinite cavity size in the span-wise direction. In order to study the grid size independency of results different grid numbers were used ranging from 95,058, 90,987 and 89,792 for rectangular, triangular and semi-circular cavities, respectively to the final control volume numbers indicated in the table 1 and it was observed that results did not change using the final control volumes indicated in table 1. The non-dimensional physical time step during the solution was 0.004 D/U_∞ in which D and U_∞ are the cavity depth and free-stream velocity (which is equal to inlet velocity), respectively. Independency of the results regarding the time step size was also under consideration. For this reason, three different physical time steps were applied for solution including of 0.04 D/U_∞, 0.008 D/U_∞ and 0.004 D/U_∞ while the value of stream-wise velocity, u, inside the shear layer within the cavities was under consideration. It should be noted that the

independency of results from grid size as well as time step was studied for each cavities, distinctly. The grid size and time step independency studies revealed rather slight differences for stream-wise velocity values. Thus, the last grid sizes (indicated in the table 1) and time step of 0.004 D/U_∞ were adopted during the present study. The convergence of the numerical 3D velocity field was established by controlling the residuals by setting its variation less than 10^{-7}. Each time steps are consisted of at least 20 time intervals and totally 3,000 time steps (60,000 iterations) are performed during the solution.

4. RESULTS AND DISCUSSION

4.1 Time-averaged flow patterns within the cavities

Figure 2 illustrates time-averaged streamlines, $\langle\psi\rangle$, patterns and velocity vector, $\langle V\rangle$, colored with time-averaged stream-wise velocity values within the cavities at Re=1,000. For each cavity such as rectangular, triangular and semi-circular shapes, three different vortical structures are developed. Firstly, primary large-scale vortex (V1) is concentrated in the upper side between the upstream and downstream walls of the cavities. Secondly, a developing vortex (V2) is developed upstream side of primary vortex. Thirdly, a small corner vortex (V3) is concentrated very close to the downstream wall of cavities. Developing of the primary and developing vortices is due to flow separation from the tip of cavity. For all three shapes, the primary large-scale vortex (V1) occupied the whole upper side of the cavity. A similar result for primary large scale have reported in the experimental study of Ozlap et al. [10]. Comparison between the images of the Figure 2 reveals that due to higher rate of fluid entrainment in the region near the upstream cavity wall, the developing vortex (V2) is larger for rectangular shape, relatively. However, some investigations such as Luo et al.[18] have stated that for very large Reynolds number (supersonic flow) the developing vortex disappears for all three cavity shapes. Further examination of the Figure 2 indicates that a corner vortex (V3) is developed for different cavity shapes under consideration in this study. This corner vortex (V3) is developed at the vicinity of downstream and lower walls of rectangular cavity while for triangular cavity this corner vortex is concentrated on the lower side of the primary vortex and very close to the developing vortex. On the other hand, the results revealed no significant corner vortex (V3) for semi-circular cavity in comparison to the other cases. Despite the fact that the concentration of secondary and corner vortices may increase the heat transfer rate within the cavity, they will impose more drag on the fluid flow.

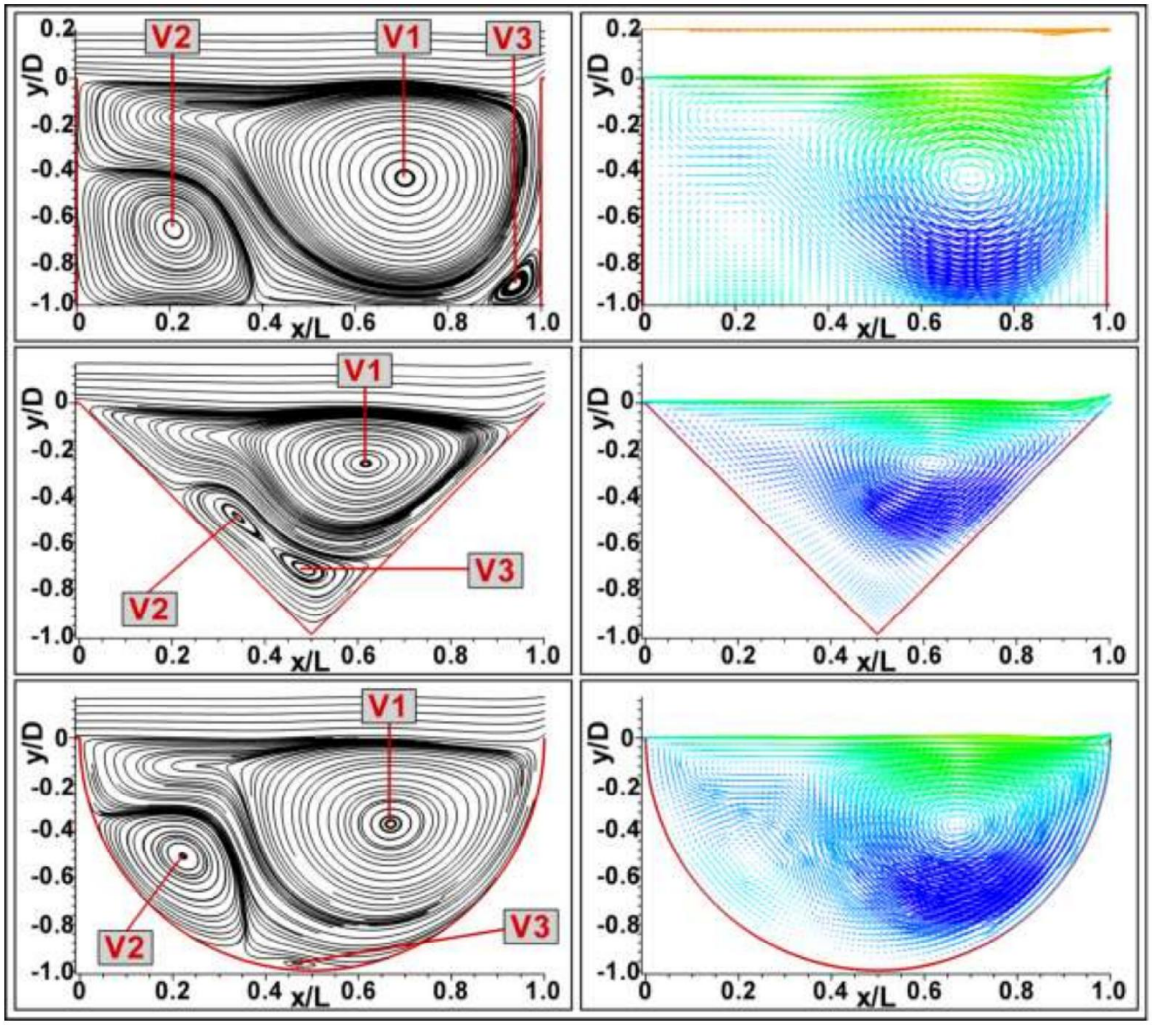


Figure 41. Time-averaged streamlines, <ψ>, patterns and velocity vector, <v>, colored with time-averaged streamwise velocity

Distributions of time-averaged stream-wise and normal velocity components, $\langle u/U_\infty \rangle$ and $\langle v/U_\infty \rangle$, are shown on the left and right hand sides of Figure 3, respectively. The values of the images in Figure 3 are normalized by free-stream velocity value as a reference velocity. It should be noted that the dashed lines indicate the negative velocity values. It can be seen clearly that a maximum negative packet of stream-wise velocity is developed for all cavity shapes. The center of mentioned pocket is approached to the downstream wall for all shapes indicating the higher rate of momentum transfer at those points in the opposite direction of free-stream motion. Comparison of the images located on the left hand side also reveals that the values of negative stream-wise velocity, $\langle u/U_\infty \rangle$, are higher for rectangular, semi-circular and triangular cavities, respectively stating the lower stream-wise fluctuating velocity within the triangular cavity. On the other hand, examination of time-averaged normal velocity, $\langle v/U_\infty \rangle$, images located at the right hand side of Figure 3 demonstrates that for all cases a pair of maximum values is concentrated within the cavity. The maximum positive part is developed at the center of cavity while the maximum negative part is approached to downstream side of the cavity. Like as the stream-wise velocity distributions, the maximum positive and negative values of normal velocity, $\langle v/U_\infty \rangle$, are higher for rectangular, semi-circular and triangular cavities, respectively indicating the lower normal fluctuating velocity concentration for triangular cavity.

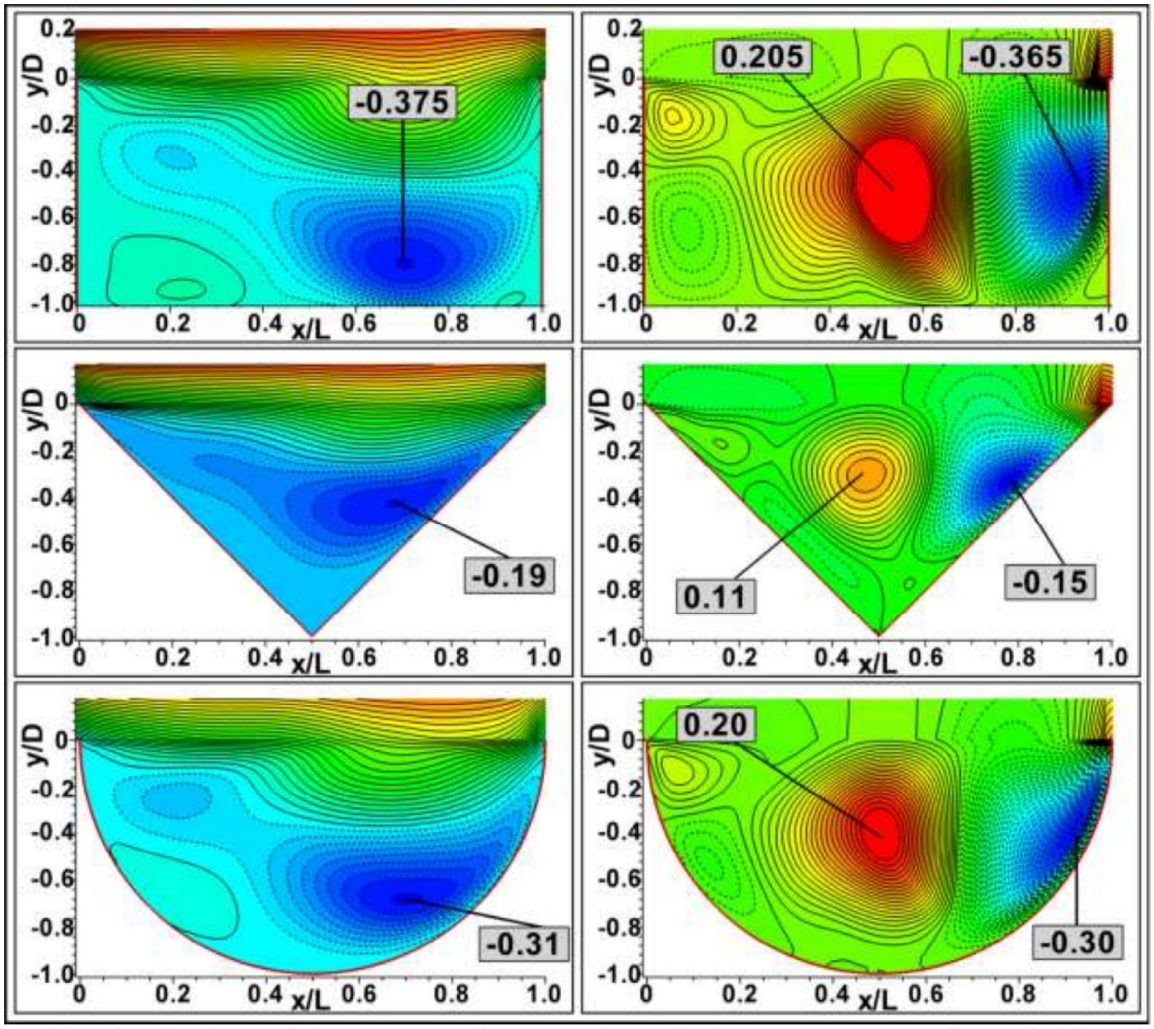


Figure 42. Distributions of time-averaged streamwise velocity component, <u/u∞> (left hand side, <δu/u∞>=0.035) and time-averaged normal velocity component, <v/u∞> (right hand side, <δv/u∞>=0.01)

In order to understand the velocity distribution within the cavities in detail, variation of stream-wise and normal velocities at different locations within the cavities are plotted in Figures 4 and 5, respectively according to the top image of Figure 4 in which the "S" is measured from the tip of cavity and "L" is the cavity length. Here, the upper row, middle row and lower row are associated with rectangular, triangular and semi-circular cavities, respectively in both Figures 4 and 5. According to the images of Figure 4 at the location of S/L=0.2, the stream-wise velocity gradient for rectangular and semi-circular cavities is higher in comparison to the triangular cavity. It is due to passing of this location across the developing vortex (V2) which rotates counter-clockwise and after that across the primary vortex (V1) which rotates clockwise for rectangular and semi-circular cavities. On the other hand, this location is completely cited inside the primary vortex (V1) for triangular case. Due to this fact, the demonstration of developing vortex (V2) for rectangular and semi-circular cavities is more significant relatively to the triangular cavity with respect to its size and effect level. At S/L=0.4, due to passing of this location from the boundary of primary and developing vortices (V1,V2) for all three cavities, the variations of stream-wise velocity are similar for all cases. Furthermore, at the locations of S/L=0.6 and 0.8, due to passing of this location across center of the negative stream-wise velocity pocket, as indicated in the left hand side images of Figure 3, the velocity gradients are high for all cases. However, this variation is relatively low for triangular cavity.

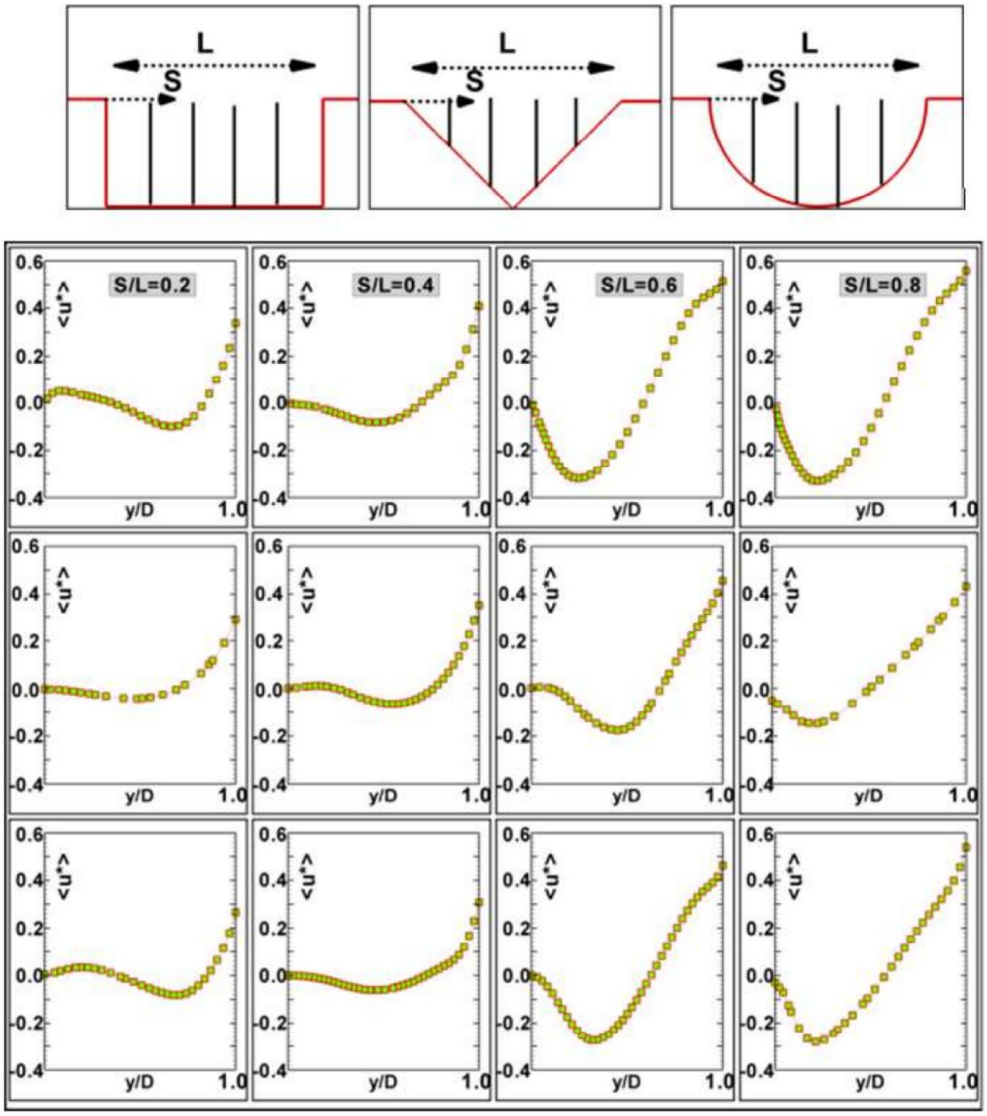


Figure 43. Variations of time-averaged streamwise velocity, <u*>= <u/u∞> at different vertical location such as s/l=0.2, 0.4, 0.6 and 0.8 inside the cavities according to the top image (first row: rectangular cavity, second row: triangular cavity, third row: semi-circular cavity)

Comparison of normal velocity, <v/U∞>, variations for three different cavities at the location of S/L=0.2 indicates no significant variations. However, at S/L=0.4 the variation of normal velocity, <v/U∞>, increases for all cavity shapes. It is due to passing of this location across the closed region to the maximum positive normal velocity zone as indicated in the right hand side images of Figure 3. At S/L=0.6, the normal velocity variation is higher and completely positive for rectangular and semi-circular cavities while there is no significant variation for triangular cavity due to passing across boundary of the maximum positive and maximum negative zones for the triangular case. Finally, due to passing across the closed region to the maximum negative zone of normal velocity, <v/U∞>, at S/L=0.8 the higher negative velocity variations are demonstrated for all cases.

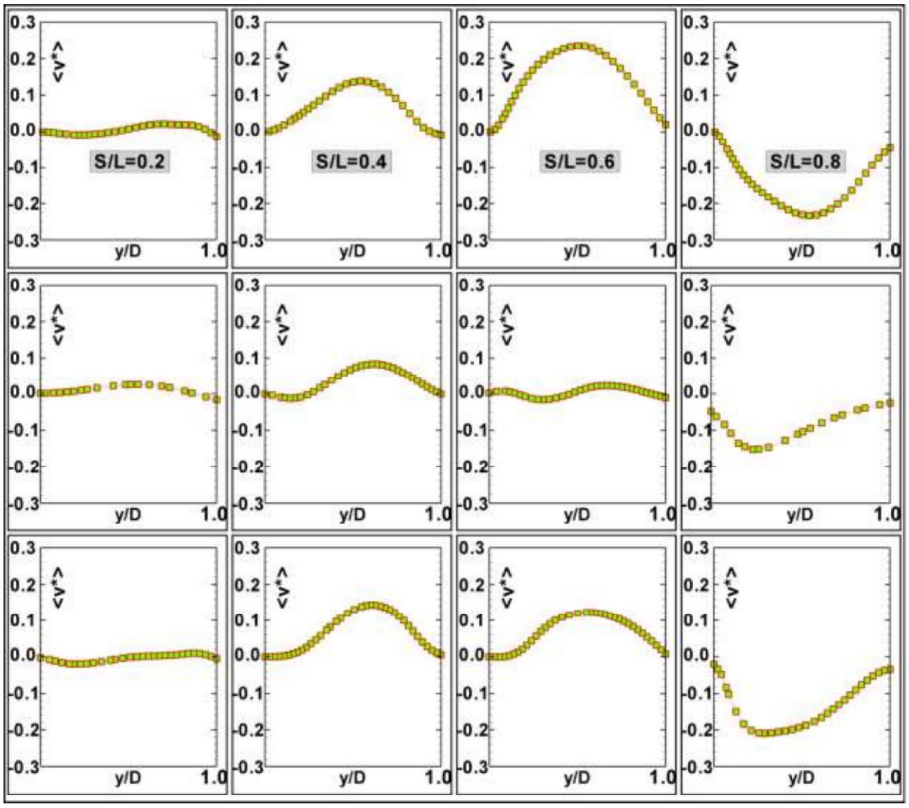


Figure 44. Variations of time-averaged normal velocity, $\langle v^* \rangle = \langle v/U_\infty \rangle$, at different vertical location such as S/L=0.2, 0.4, 0.6 and 0.8 inside the cavities according to the top image of Fig. 4 (first row: rectangular cavity, second row: triangular cavity, third row: semi-circular cavity)

One of the encountered problem about the flow within cavities is the imposed drag on the fluid motion by cavities. At the end of this subsection, we will consider the static pressure distribution within the three different cavities. Figure 6 demonstrates time-averaged non-dimensional pressure, $\langle P_s/0.5\rho U^2_\infty \rangle$, within all cases of cavity in which the P_s is the dimensionless static pressure that has been scaled by dynamic pressure, $0.5\rho U^2_\infty$. Examination of the indicated images reveals that for each case a pair of maximum and minimum pressure is developed between the center of cavity and its downstream wall for all cases. The maximum positive pressure zone is very close to the trail of cavities. The significant appearance of the positive pressure is due to separation of flow at the trailing edge of cavities as well as the large difference between the velocities of free-stream and within the cavities. Upstream of the positive zone, the maximum negative zone of pressure is developed for all cavity shapes. The concentrated negative pressure zone is more significant than its positive zone. This negative zone is the main cause for drag imposing. Further examination reveals that the value of maximum negative pressure for triangular cavity is less than the other cases which indicates the less drag imposing on the flow. After the triangular cavity, semi-circular cavity has lower value of maximum negative pressure in comparison to rectangular cavity.

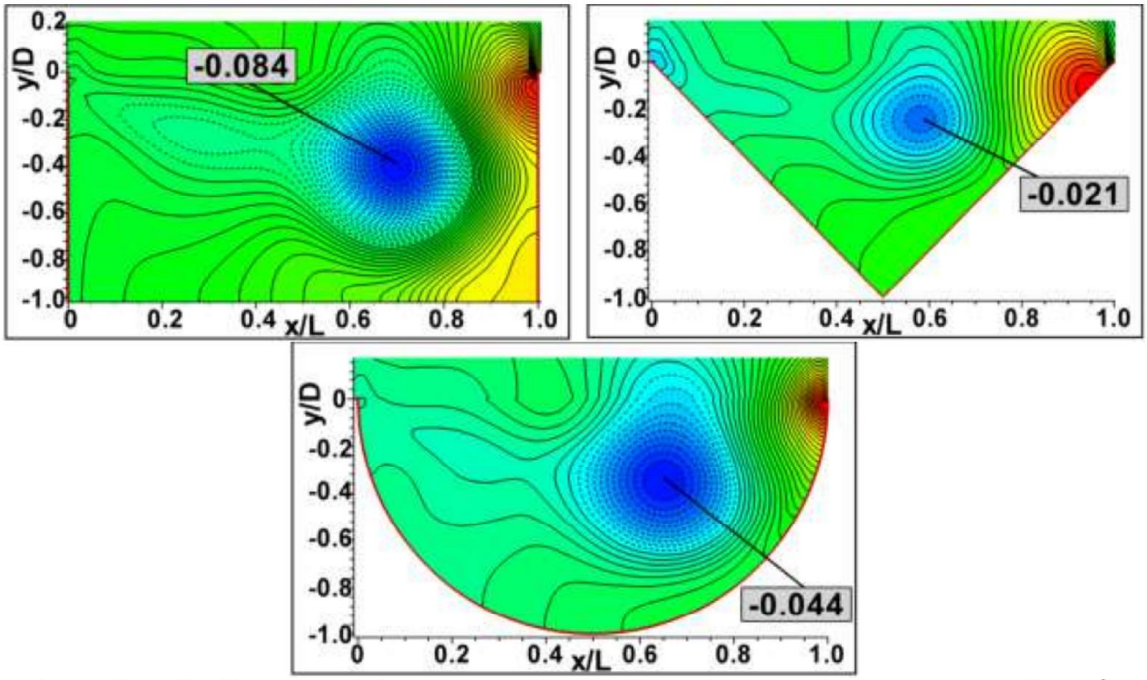


Figure 45. Distributions of time-averaged non-dimensional static pressure, $<p_s/0.5\rho u^2_\infty>$ ($<\delta p_s/0.5\rho u^2_\infty>=0.004$)

4.2 Instantaneous flow patterns within the cavities

It is known that time-averaged flow data do not provide the details of flow behavior. For this reason, one can study and analyze the flow characteristics by instantaneous flow data. We have provided the instantaneous flow patterns in Figure 7 in order to reveal the flow behavior in details.

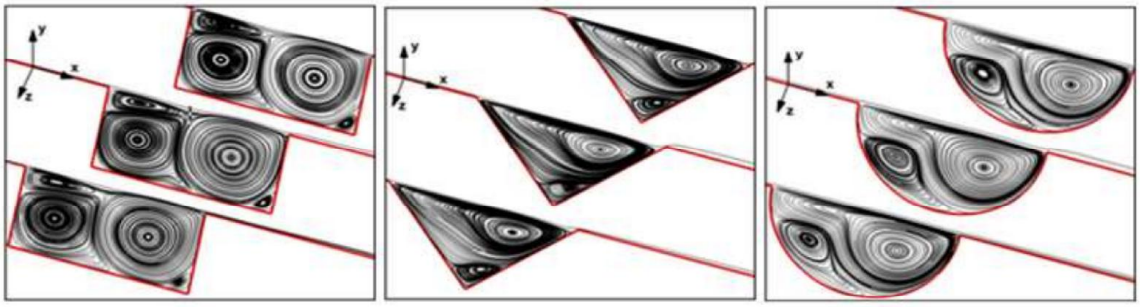


Figure 46. Instantaneous streamlines, ψ, patterns at three different spanwise sections

This Figure illustrates the instantaneous streamlines, ψ, patterns at three different span-wise sections at the same time. Explanation of images of Figure 7 may be provided at two following steps:

Examination of the images of Figure 7 states that within the rectangular cavity the developing vortex (V2) gradually becomes larger for a certain period of time. This periodic appearance reveals a similar time-averaged pattern indicated in the first image of Figure 2. However, the existing of corner vortex (V3) is fixed. Within the triangular cavity, the developing vortex (V2) disappears time to time and forces the corner vortex (V3) to approach to the downstream wall. On the other hand, flow behavior within the circular cavity does not change significantly. Further examination of flow behavior by numerical animation indicates that the rate of unsteadiness within the cavity at Re=1,000 is low for semi-circular, triangular and rectangular cavities, respectively. However, the rate of this unsteadiness may be changed by varying the Reynolds number or aspect ratio of cavities.

Examination of flow patterns within the three span-wise section states that due to the same flow pattern at different span-wise direction and unchanged flow data, flow is completely two-dimensional. In another words, flow characteristics change in stream-wise and normal directions and they do not change in the span-wise direction. It is because of long length of cavities in the span-wise direction, symmetrical boundary conditions assumption for sides of cavity and relatively lower Reynolds number.

5. CONCLUSION

Numerical computations of shear driven vortex flow within the three different cavities such as rectangular, triangular and semi-circular shapes were investigated using SST k-ω turbulence model at Re=1,000. Examination of time-averaged flow patterns revealed that three different vortex mechanisms dominate for all under consideration cavities. The primary vortex (V1) which is the larger one dominates between the upstream and downstream walls of cavities. Secondary or developing vortex (V2) is developed in the upstream side of the primary vortex at the region very close to the upstream wall of cavities. Finally, a small corner vortex (V3) is developed at the vicinity of downstream and lower wall of cavities. It is found that rate of unsteadiness within the rectangular cavity is more than triangular and semi-circular cavities. Furthermore, rectangular cavity imposes more drag on the fluid motion. On the other hand, using of SST k-ω turbulence model satisfies the previous results that have used the other turbulence models. Finally, it is obtained that flow within the rectangular, triangular and semi-circular cavities with infinite length in span-wise direction, is two-dimensional in stream-wise and normal directions at Re=1,000.

ACKNOWLEDGMENTS

The authors would like to acknowledge the funding of the Research Projects Office of Cukurova University under contract No: MMF 2012D17.

REFERENCES

Zhang, T., Shi, B., Chai, Z.: Lattice Boltzmann simulation of lid-driven flow in trapezoidal cavities. *J. Computers and Fluids.* 39, 1977-1989 (2010)

Povitsky, A.: Three-dimensional flow in cavity at yaw. *J. Nonlinear Analysis.* 63, 1573-1584, 2005.

Oueslati, F., Ben Beya, B., Lili, T.: Aspect ratio effects on three-dimensional incompressible flow in a two-sided non-facing lid-driven parallelepiped cavity. *J. Comptes Rendus Mecanique.* 339, 655-665, 2011.

Guermond, J.L., Migeon, C., Pineau, G., Quartapelle, L.: Start-up flows in a three-dimensional rectangular driven cavity of aspect ratio 1:1:2 at Re = 1000. *J. Fluid Mechanics.* 450: 169-199, 2002.

Vasseur, P., Robillard, L., Anochiravani, I.: Natural convection in a shallow porous cavity heated from the side with a uniform heat flux. *J. Chemical Engineering Communications.* 46: 129-146, 1986.

Stefanovic, D.L., Stefan, H.G.: Simulation of transient cavity flows driven by buoyancy and shear. *J. of Hydraulic research.* 38, 181-195, 2011.

Zdanski, P.S.B., Ortega, M.A., Fico Jr, N.G.C.R.: On the flow over cavities of large aspect ratio: A physical analysis. *J. International Communications in Heat and Mass Transfer.* 33, 458- 466, 2006.

Saqr, K.M., Aly, H.S., Kassem, H.I., Mohsin, M.S., Wahid, M.A.: Computational of shear driven vortex flow in a cylindrical cavity using a modified k-ε turbulent model. *J. International Communications in Heat and Mass Transfer.* 37, 1072-1077, 2010.

Mesalhy, O.M., Abdel Aziz, S.S., El-Sayed, M.: Flow and heat transfer over shallow cavities. *J. Thermal Science.* 49, 514- 521, 2010.

Ozalp, C., Pinarbasi, A., Sahin, B.: Experimental measurement of flow past cvities of different shapes. *J. Experimental Thermal and Fluid Science.* 34, 505- 515, 2010.

Ho, C.J., Lin, F.H.: Numerical simulation of three-dimensional incompressible flow by a new formulation. *Int. J. for Numerical Methods in Fluids.* 23, 1073–1084, 1996.

Wei, J.J., Yu, B., Tao, W.Q., Kawaguchi, Y., Wang, H.S.: A new high-order-accurate and bounded scheme for incompressible flow. *Numerical Heat Transfer, Part B: Fundamentals.* 43, 19–41, 2003.

Gupta, M.M., Kalita, J.C.: New paradigm continued: further computations with streamfunction-velocity formulations for solving Navier–Stokes equations. *Communications in Applied Analysis.* 10, 461–490, 2006.

Peng, S.H., Davidson,L.: Large eddy simulation for turbulent buoyant flow in a confined cavity. *Int. J. Heat and Fluid Flow.* 22, 323-331, 2001.

Diang, H., Shu, C., Yeo, K.S., Xu, D.: Numerical computation of three-dimensional ncompressible viscous flows in the primitive variable form by local multiquadric differential quadrature method. *Computer Methods in Applied Mechanics and Engineering.* 195, 516–533, 2006.

Menter, F.R.: Two-Equation Eddy-Viscosity Turbulence Models for Engineering Applications. *AIAA Journal.* 32, 1598-1605,1994.

Dewan, A.: Tackling Turbulent Flows in Engineering. Springer, Verlag Berlin Heidelberg, 2011.

Luo, S.B., Huang, W., Liu, J. Wang, Z.G.: Drag force investigation of cavities with different geometric configurations in supersonic flow. *Science China Technological Science.* 54(5), 1345-1350, 2011.